

A FEM-BASED MODEL TO STUDY THE BEHAVIOR OF SRG-STRENGTHENED R/C BEAMS

Antonios A. Katsamakas ¹, Vassilis K. Papanikolaou ² and Georgia E. Thermou ³

¹ PhD student, Chair of Seismic Design and Analysis, ETH Zurich,
Zurich, CH-8093, Switzerland

² Assistant Professor, School of Civil Engineering, Aristotle University of Thessaloniki,
Thessaloniki, GR-54124, Greece.

³ Assistant Professor in Structural Engineering, The University of Nottingham,
Nottingham, NG7 2RD, UK.

Abstract. In this paper, a new time-effective modeling approach is proposed for predicting the response of shear-deficient reinforced concrete (R/C) beams strengthened with steel-reinforced grout (SRG) jackets. Solid finite elements are utilized for concrete using a fracture-plasticity constitutive law, while both high-strength steel cords and conventional reinforcement are modeled using embedded truss elements with multilinear stress-strain laws. The efficiency of the proposed method is assessed by comparing numerical against experimental data of nine shear-deficient beams strengthened with various SRG jacketing configurations. The comparison demonstrated close correlation both in terms of failure mode and force-displacement curves. The numerical analysis predicted the observed crack pattern and failure modes accurately, whereas deviation in terms of load and deflection was, on average, less than 1 % and 10 %, respectively.

Keywords. SRG; textiles; finite elements; strengthening; retrofitting; composite materials; shear; beams; reinforced concrete.

1. INTRODUCTION

Over the last decades, the increased need for retrofitting of existing reinforced concrete (R/C) structures led to the development of composite materials used as externally bonded reinforcement, such as Fiber Reinforced Polymers (FRPs) (e.g. [1-12]). The favorable mechanical properties of FRPs (i.e. high tensile strength, high strength-to-weight ratio, corrosion resistance, easy and fast application) led to their widespread use in strengthening applications of R/C and masonry structures. However, the use of resin as the connecting material (binder) between the concrete substrate and the composite fabric has several shortcomings (i.e. poor bonding at elevated temperatures, challenging application on wet surfaces or at low temperatures and insufficient performance under fire conditions). Therefore, the recent use of mortar binders instead of resins led to the development of the new generation of inorganic composite materials, named Fibre-Reinforced Cementitious Matrix (FRCM), e.g. [13-34]. Specifically, Steel Reinforced Grout (SRG), belonging to the FRCM family of composite materials, is a relatively new composite system that comprises high strength steel textiles embedded in cementitious grout. Past experimental studies have demonstrated the efficiency of SRG in increasing strength and deformation capacity of plain concrete and R/C members such as columns, slabs, and beams [13, 23-34].

Recent experimental studies have revealed the efficiency of the SRG jacketing technique in alleviating deficiencies related to shear critical beams. Gonzales-Libreros et al. (2017) [31] tested shear-deficient R/C beams, investigating the influence of the jacketing material (i.e. SRG, carbon FRCM, steel FRP or carbon FRP). Experimental results have demonstrated that the shear strength of the beams increases proportionally to the axial stiffness of the retrofitting jacket and is unaffected by the type of the utilized matrix (i.e. cementitious or resin). For SRG-strengthened beams, load increase was within the range of 20-30 %. Wakjira and Ebead (2019) [32] tested R/C T-cross-section beams. The main investigated parameters were the steel

textile density and the bond scheme (i.e. side bonded and U-wrapped). Results concluded that the U-shaped jacketing bond scheme was more effective than the side bonded, and that increasing the density of the textile leads to strength increase. The shear capacity of the jacketed beams, when compared to the control ones, increased from 10 % to 71 %. In a recent study, Thermou et al. (2019) [30] tested eleven shear-critical R/C beams, where two of them served as control specimens, whereas the rest were strengthened with different SRG jacketing configurations. The application of the SRG jackets substantially increased the load (up to 160 %) and deflection capacity (up to 450 %) of the retrofitted beams. Since the experimental results of this study are utilized to evaluate the proposed numerical model, a description of the experimental investigation will follow in the next section.

In general, finite element analysis of externally applied composite reinforcement, combined with inorganic binders, for retrofitting of structural elements (beams or columns) is very limited in the literature. To the best of authors' knowledge, the only FEM-based investigation of SRG-retrofitted R/C beams is the one conducted by Bencardino and Condello (2016) [35] who simulated five flexure-deficient beams using the general-purpose finite element software Abaqus. The corresponding experimental results were utilized to calibrate the numerical simulation and assess its efficiency. The main objective of the study was the proposal of an inelastic three-dimensional finite element representation, able to predict the response of R/C beams strengthened in flexure with steel-based strips. Parameters of the investigation were the type of the matrix (i.e. grout and resin for the SRG and SRP strips, respectively) and the anchorage system (i.e. U-wrapped at the end of the beam's length or none). The first specimen was the control specimen, two specimens were retrofitted using SRG or SRP strips at the tension face of the beam, without anchors, and the last two specimens were strengthened with similar strips comprising U-shaped anchorages at the end of the strip length. The concrete, internal steel bars and external reinforcement were modeled using tetrahedron, truss and shell

elements, respectively. The selected material for concrete was of damage-plasticity type, where tensile cracking and compressive crushing are assumed as the principal failure mechanisms. Compressive behavior followed Hognestad's simplified stress-strain equation, whereas tensile response was linear elastic up to failure. The constitutive law utilized for longitudinal and transverse steel reinforcement was bilinear elastic-perfectly plastic. Even though both SRG and SRP materials are naturally orthotropic, their mechanical behavior was represented as isotropic. Cohesive surfaces were utilized to simulate the bond between concrete and SRG/SRP systems. The bond-slip equation that characterized the surfaces mentioned above was the FRP-concrete law developed by Yuan et al. (2012) [36]. Experimental results demonstrated that the load error was up to 14 %, whereas, for the corresponding displacement error, up to 32.8 %. The simulation was generally unable to reproduce the load-deflection curve after the peak load (i.e. post-peak behavior).

In the present paper, an 'explicit' finite element representation is proposed to predict the response of R/C beams, strengthened with SRG jackets. Concrete is typically modeled with three-dimensional finite elements with a nonlinear material constitutive law, while reinforcement is represented with embedded trusses in the concrete solid elements. A new approach for modeling external SRG jackets is herein suggested, where the high strength steel textile is explicitly modelled using individual cords as embedded truss elements, promoting time-efficiency, accuracy and robustness, as well as clarity and consistency with the physical problem. Numerical analysis was able to accurately predict the beam failure mode, also showing low deviations between experimental and numerical results in terms of load and deflection (less than 1 % and 10 %, respectively).

2. EXPERIMENTAL INVESTIGATION OF SHEAR CRITICAL BEAMS

2.1 Experimental program

In order to evaluate the efficiency of the proposed modeling approach, the results of a recent experimental investigation by Thermou et al. (2019) [30] were utilized for comparisons against numerical results. Eleven R/C beams were tested under three-point bending, while the main parameters of investigation were the jacketing configuration (U- and fully-wrapped), the density of the high strength steel textile (1.57 and 4.72 cords/cm) and the number of the layers of the SRG jacket (one and two).

The R/C beams were intentionally designed as short, with a clear span-to-depth ration equal to $a/d = 2.2$, to promote shear failure. The width and height of the cross-section of the beams were equal to 200 mm and 300 mm respectively, whereas the total length was equal to 2000 mm. Specimens were divided into two groups (A and B), based on the longitudinal steel reinforcement ratio (Table 1). Group A comprised five beams; one of them serving as control (i.e. no strengthening was applied) and four beams with different jacketing configurations. These specimens had 4 \varnothing 12 mm steel bars placed at the corners of the section as longitudinal reinforcement (Figure 1). Group B contained one control and five SRG-strengthened beams, which comprised 4 \varnothing 16 mm and 2 \varnothing 10 mm steel bars as bottom and top longitudinal reinforcement, respectively (Figure 1). All specimens were subjected to three-point bending tests. Beams from both groups included \varnothing 8 mm closed stirrups placed at a uniform spacing of 100 mm along a span of 1100 mm, leaving the remaining 600 mm without any transverse reinforcement. The control specimens were designed to fail in shear with the damage localized in the critical region of 600 mm (no stirrups) (Fig. 1). Alternative SRG jacketing configurations were applied along the 600 mm to assess the the efficiency of the new composite system to alleviate deficiencies. The mean concrete compressive strength (f_{cm}) was 28 MPa and 23.3 MPa

for Group A and Group B specimens, respectively. The steel grade used both for longitudinal and transverse steel reinforcement was B500C.

Specimens were given the notation XYZW, where X indicates the group of the tested beam (i.e. Group A or B), and Y represents the type of the jacketing system (i.e. 0 for the control specimens, U for the U-wrapped jacket and F for the fully-wrapped jacket). Z indicates the density of the steel textile (i.e. L for the low-density 1.57 cords/cm textile and H for the high-density 4.72 cords/cm textile, Fig. 2(a)), whereas W corresponds to the number of layers (1 or 2, for the single and double-layered SRG jackets, respectively, Fig. 2(b)).

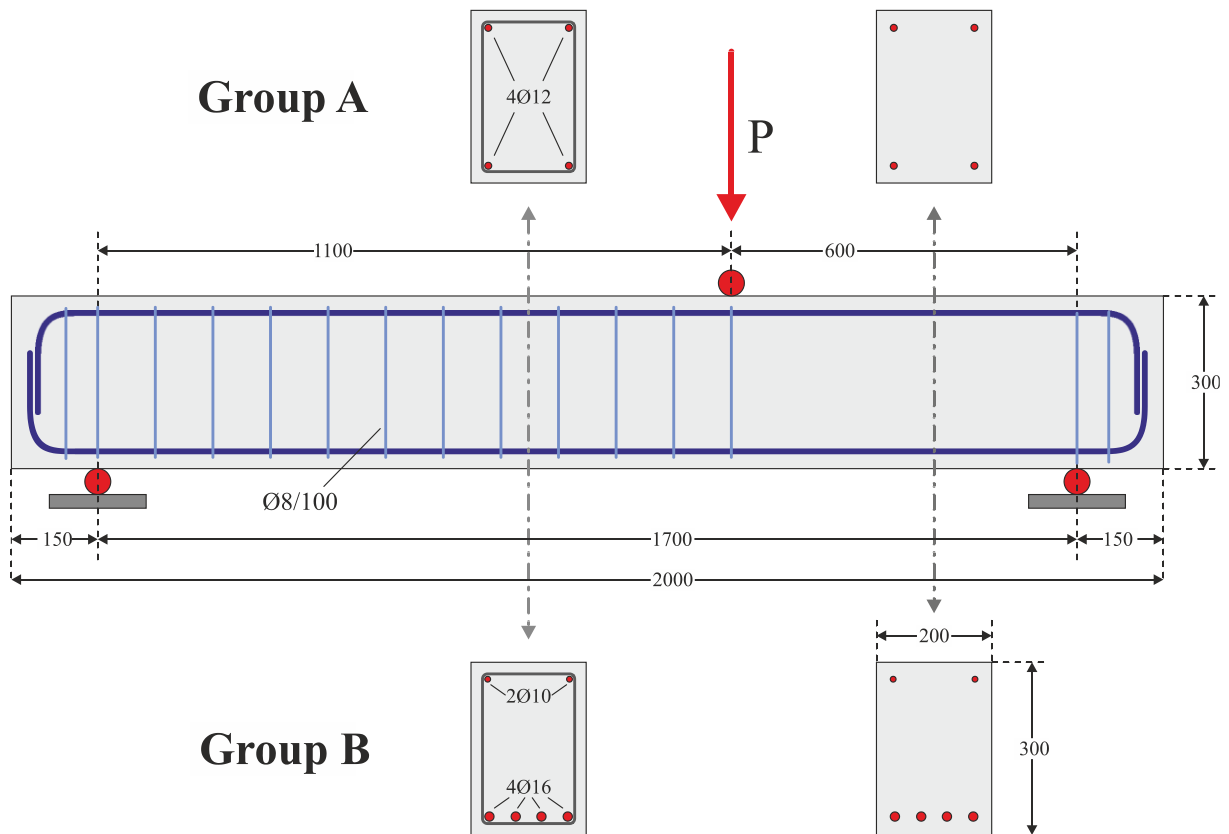


Figure 1: Geometry and reinforcement details of Group A and Group B specimens, as tested experimentally by Thermou et al. (2019).

A three-point bending setup was configured, where the R/C beam was simply supported on a pair of freely-rotating steel rods. The vertical load was applied by a 1000 kN compression capacity actuator monotonically, whereas displacement was externally measured using a draw-wire sensor placed underneath the beam, directly below the load application point.

Table 1. Details of specimens in the experimental investigation by Thermou et al. (2019)

| Group | Name | f_{cm} (MPa) | Jacket type | Textile density (cords/cm) | Jacket layers |
|----------|------|----------------|---------------|----------------------------|---------------|
| A | A0 | 28.0 | None | – | – |
| | AUH1 | | U-wrapped | 4.72 | 1 |
| | AFL1 | | Fully-wrapped | 1.57 | 1 |
| | AFH1 | | Fully-wrapped | 4.72 | 1 |
| B | B0 | 23.3 | None | – | – |
| | BUL1 | | U-wrapped | 1.57 | 1 |
| | BUL2 | | U-wrapped | 1.57 | 2 |
| | BFL1 | | Fully-wrapped | 1.57 | 1 |
| | BFL2 | | Fully-wrapped | 1.57 | 2 |

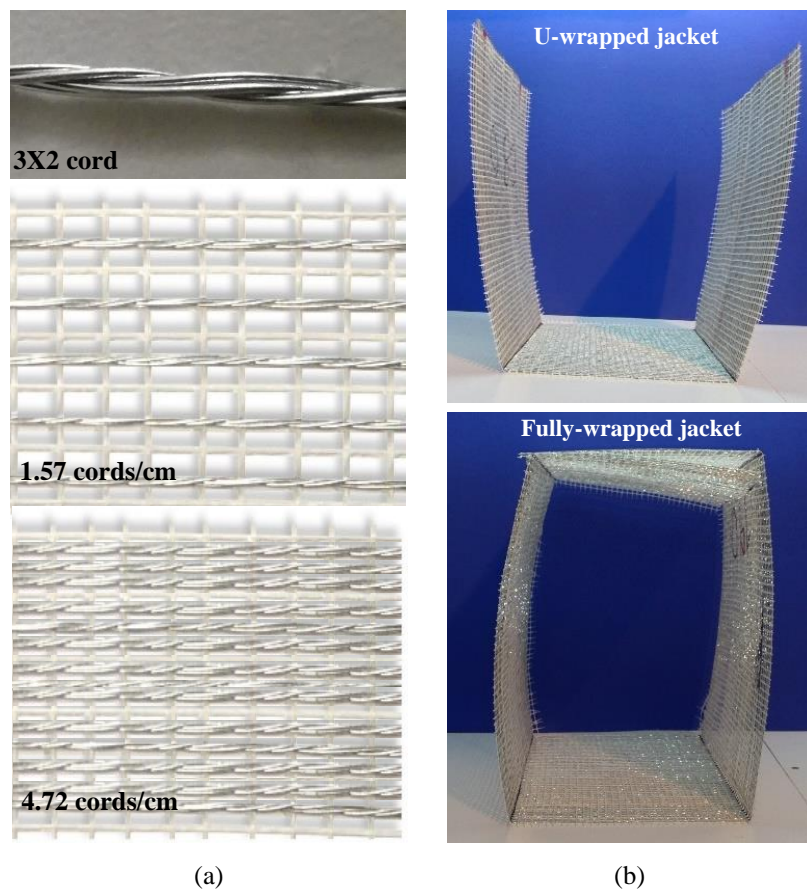


Figure 2. (a) Single steel cord and different densities of the utilized steel textile; (b) Preparation of the steel textile before the application.

2.2 Test results

Test results demonstrated the efficiency of SRG jacketing in increasing both strength (up to 160 %) and deformation capacity (up to 450 %) of the shear critical beams. For Group A, the alternative jacketing schemes had a similar effect. All jacketing configurations applied to specimens of Group A increased the peak load and deformation capacity by up to 38 % and 12 %, respectively. Moreover, the failure mode transitioned from shear to flexural failure. For Group B specimens, the jacketing configuration had a significant impact on the results; U-wrapped SRG jackets managed to increase the maximum load and deflection at the ultimate load up to 109 % and 73 %, respectively. Fully-wrapped jackets managed to increase strength up to 160 %, but, most importantly, accomplished to shift the failure mode from brittle (shear) to ductile (flexure). Moreover, fully-wrapped jackets failed due to tensile fracture of the cords, hence developed their full strength. The experimental force-displacement curves are presented along with their numerical counterparts in the next section (Figs. 7, 8). More details regarding the experimental response of the SRG jacketed beams can be found in Thermou et al. [30].

3. NUMERICAL ANALYSIS

3.1 General

For modeling and analysis of the above SRG-jacketed R/C beams, finite element software ATENA [37-39] was selected, based on the following criteria [40-42]:

1. Availability of robust and mesh-independent nonlinear constitutive models for concrete.
2. Ability to model steel reinforcement using embedded (instead of discrete) truss elements.
3. Availability of reliable convergence algorithms and nonlinear solvers for deriving the softening branch of the response.

To evaluate the efficiency of the proposed numerical approach, the numerical results were compared with the experimental ones, employing the criteria of (a) similarity of failure modes

based on cracking patterns and (b) correlation between experimental and numerical response (force-displacement) curves, as well as energy dissipation capacity.

3.2 A new modeling approach for SRG jacketing

Previous studies [35] and software guides [39] generally suggest the use of isotropic two-dimensional plane stress elements to model externally applied fabric jackets (e.g. FRP). This approach considers a 3D solid element concrete beam model, where a jacket, modeled by 2D plane stress elements, is superimposed on concrete through an intermediate (auxiliary) surface. The concrete beam is connected to this auxiliary surface using a fixed contact, whereas the auxiliary surface is connected to the external jacket using an interface volume element [38]. It is worth noting that the above auxiliary surface has no physical representation and is only utilized to impose mesh compatibility between concrete and fabric. Through trial analyses, this approach was found to have several shortcomings, such as complexity, time-inefficiency and, most importantly, the inability to accurately reproduce the experimentally observed behavior. These disadvantages are summarized as follows:

1. The auxiliary surface is modeled using an elastic material. Therefore, parameters such as the elastic modulus and Poisson's ratio should be selected. Assuming a reasonable value for Poisson's ratio (i.e. 0.2), it is evident that the elastic modulus still remains the critical parameter. By using a relatively high value for this parameter makes the auxiliary surface stiff enough to absorb all stress, eventually transferring extremely low stresses to the jacket plane, and making the analysis unable to predict the jacket failure mode. On the other hand, using a low value for the elastic modulus makes the auxiliary surface too deformable and the member eventually behaves as non-retrofitted. Intermediate values do not significantly mitigate the above issue.
2. The use of isotropic two-dimensional elements for the fabric suggest that coupling exists between the two orthogonal axes, expressed by the Poisson's ratio. This interaction

contradicts the physical behavior of the applied SRG textiles, which comprise unidirectional steel cords.

3. Creating a large number of surfaces and contact conditions significantly increases the computational cost.

Considering the above disadvantages, a new modeling approach was applied for SRG jackets, where steel cords are individually represented by 2-node truss elements embedded in the concrete volume (Figure 3). In the case of fully-wrapped SRG jackets, perfect bond between cords and mortar was considered (zero slip) since the cross section is well confined by the fully-wrapped jackets with sufficient anchorage length; thus, demonstrate zero slippage. Contrariwise, for U-wrapped jackets, the *fib* MC 2010 [44] bond-slip equations were adopted, since slippage is expected to occur in this jacketing type. It is noted that the introduction of the direct embedment of individual steel cords into concrete, neglecting the presence of the cementitious matrix, greatly simplified the modeling process. As a result, any bond behavior between the fibers and the matrix as well as the matrix and the substrate is now *smeared* into the adopted bond-slip law for U-wrapped jackets. The *fib* MC 2010 [44] bond-slip model was employed in lack of the existence of a bond-slip model exclusively derived for SRG systems. The numerical results showed that this initial assumption was reasonable. It is in the authors' intention to refine the proposed numerical approach by adopting bond-slip laws representative of the SRG composite systems in future studies.

Through the proposed modeling approach, the number of utilized finite elements and solution time was reduced by 50 % and 80 %, respectively. For instance, the number of finite elements was reduced from approximately 50.000 to 25.000, whereas the solution time from 10 to only 2 hours on a medium-performance computer. The employed constitutive laws and finite elements are presented in the following sections.

3.3 Material constitutive laws

3.3.1. Concrete

The selected three-dimensional constitutive law for concrete (NonLinCementitious2) can describe failure modes both in tension and compression. Specifically, it combines fracture in tension with plasticity in compression [43]. Fracture is simulated by an orthotropic smeared crack formulation and a mesh-independent crack band model, based on the Rankine tensile criterion with exponential softening [42]. The plasticity hardening-softening model for concrete in compression is based on the Men etrey-Willam three-parameter failure surface [45, 46] and a non-associated flow rule of Drucker-Prager type. Strains are separated into elastic, plastic and fracturing components and a recursive iterative algorithm combines these components by preserving stress equivalence. The algorithm can also handle cases when failure surfaces of both models are active or when physical changes occur, such as crack closure [38].

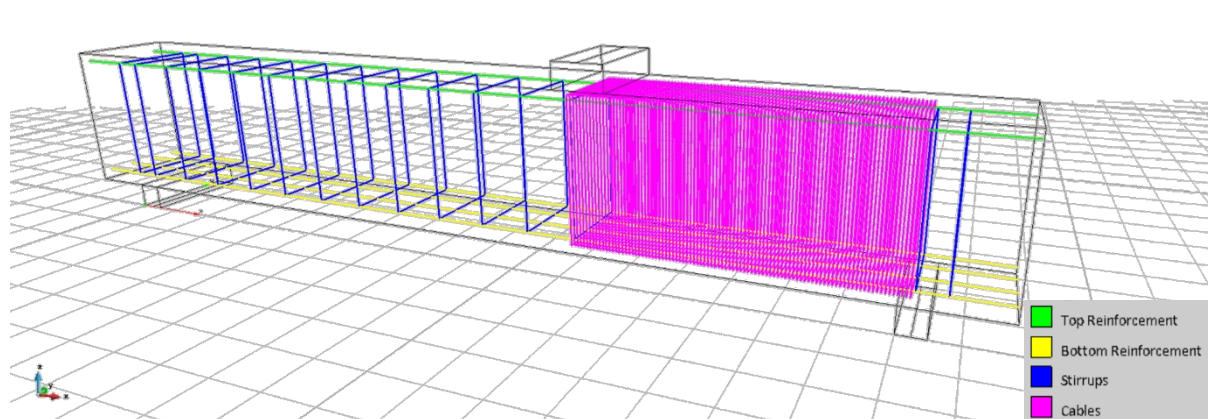


Figure 3. Schematic representation of the suggested modeling approach for the externally applied textile.

The existing constitutive law for concrete was calibrated based on the experimental results of Thermou et al. [30] (Table 2). A constant shear factor (S_F) defining the ratio between shear and normal crack stiffnesses was used, with lower values leading to reduced concrete shear strength. Through pilot analyses, it was observed that the overall shear strength is moderately dependent on the shear factor. A shear factor value equal to 15 was calibrated for control beams

(A0 and B0) and to 10 for all strengthened specimens (AUH1, AFL1, AFH1, BUL1, BUL2, BFL1, BFL2). The concrete constitutive law was modified to reflect the effect of confinement in the case of fully-wrapped jackets . Specifically, plastic strain and critical compressive displacement were increased from 0.002 (default) to 0.005 and from 5 mm (default) to 10 mm, respectively. This increase is generally justified by the nature of the confinement action, where concrete strain and strength increases; these specific values were the outcome of the model calibration. For all other model parameters, the default values were used, as described in [38].

Table 2. Selected values for various parameters affecting concrete behavior.

| | Group A | Group B |
|--|-----------------------|-----------------------------|
| Compressive strength (MPa) | 28 | 23.3 |
| Tensile strength (MPa) | 2.1 | 1.7 |
| Poisson's Ratio (-) | 0.2 | 0.2 |
| Elastic modulus (GPa) | 30 | 29 |
| Plastic strain (-) | 0.005 (AFL1, AFH1) | 0.005 (BFL1, BFL2) |
| | 0.002 (A0, AUH1) | 0.002 (B0, BUL1, BUL2) |
| Shear factor | 15 (A0) | 15 (B0) |
| | 10 (AFL1, AFH1, AUH1) | 10 (BFL1, BFL2, BUL1, BUL2) |
| Critical compressive displacement (mm) | 10 (AFL1, AFL2) | 10 (BFL1, BFL2) |
| | 5 (A0, AUL1, AUL1) | 5 (B0, BUL1, BUL1) |
| F _c reduction (-) | 0.5 | 0.5 |
| Fracture Energy (N/m) | 131 | 124 |
| Eccentricity (-) | 0.52 | 0.52 |
| Direction of plastic flow (-) | 0 | 0 |

3.3.2. Steel reinforcement

The constitutive law utilized for reinforcement is based on a uniaxial multilinear law, enabling to trace all stages of steel behavior, both elastic and inelastic [42]. The selected stress-strain diagram corresponds to steel grade B500C (the properties assigned are the same as the steel utilized in the experimental investigation) and is illustrated in Figure 4. The yield stress, the maximum stress, the yield strain and the maximum strain were equal to $f_y = 530$ MPa,

$f_u = 600$ MPa, $\varepsilon_y = 0.00265$, and $\varepsilon_u = 0.075$, respectively. The reinforcement was embedded in the concrete volume. Perfect bond between steel reinforcement and concrete was assumed since adequate anchorage length was provided.

3.3.3. SRG

High strength steel cords were modeled individually, using a similar constitutive law to reinforcement (i.e. embedded in the concrete volume). The bilinear stress-strain diagram appears in Figure 4 and is identical to the stress-strain diagram of the steel cords utilized in the experimental investigation. The maximum stress and the corresponding strain, measured experimentally, were set to $f_u = 2800$ MPa and $\varepsilon_u = 0.01474$, respectively. Note that for the steel cords the elastic modulus is slightly lower than common steel ($E = 190$ GPa). The minor tensile strength of the inorganic matrix was ignored, and only adhesion between cords and the R/C beam was considered. In the case of the fully-wrapped jackets (specimens AFL1, AFH1, BFL1, BFL2), full bond between the cords and the beam was adopted. The *fib* MC 2010 [44] bond-slip law was applied on the cords' endpoints of the U-wrapped jackets (specimens AUH1, BUL1, BUL2). From the available options in *fib* MC 2010 [44], the bond was considered as “Good,” and the corresponding default values were selected.

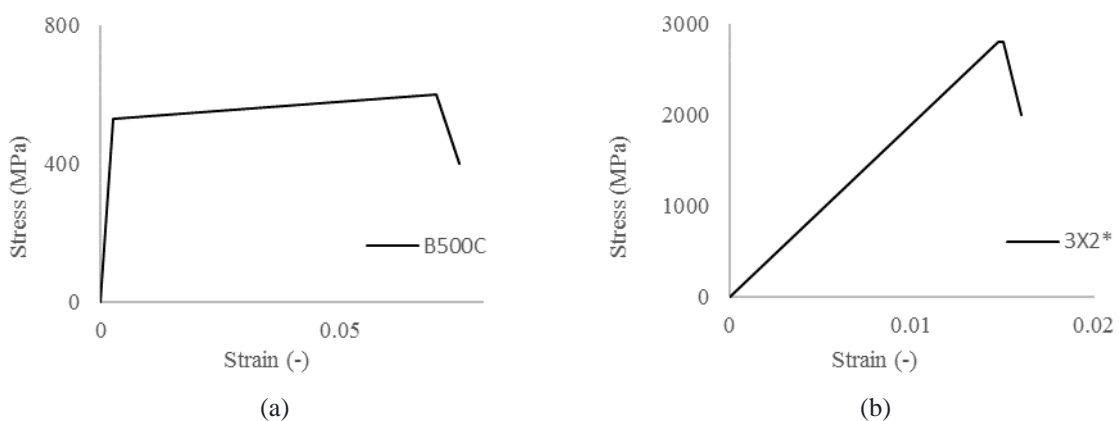


Figure 4. (a) Simplified stress-strain diagram in tension of internal steel reinforcement; (b) steel cords.

3.4 Finite element modeling and analysis procedure

Concrete was modeled using 8-node isoparametric solid (brick) elements, with three degrees of freedom per node, comprising eight integration points, with each side length equal to 2 cm. Pilot studies proved that a finer mesh neither increases accuracy nor is recommended, because it falls below the maximum aggregate size. This is also in accordance with the crack band model formulation, that exhibits no mesh sensitivity. Steel cords and reinforcement bars were modeled by 2-node truss elements, with one axial degree of freedom per node, having two integration points.

The load was applied as prescribed displacement in small increments in order to simulate the experimental procedure and favor convergence. To evaluate the force-displacement response curves of the specimens, two monitoring points were utilized, as per the experimental setup. The first was placed on the loading plate monitoring the applied load in terms of the reaction against the prescribed displacement, and the second was located on the bottom surface of the R/C beam, right below the first one, monitoring the corresponding displacement. The recordings of these two monitoring points were plotted together to create the force-displacement curves.

3.5 Convergence criteria

The modified Newton-Raphson (mNR) iterative scheme was applied, with appropriate convergence criteria and a maximum number of iterations. Specifically, the displacement error, the residual error, and the absolute residual error were equal to 0.005, the energy error was equal to $5 \cdot 10^{-6}$, and the maximum number of iterations was set to 200. Sloan algorithm was selected to optimize bandwidth. The elastic predictor was selected for the stiffness type, whereas the stiffness matrix was reassembled at the start of each step. From the various available solvers, Pardiso [47] was chosen. Pilot studies proved that further refinement of the

parameters mentioned above did not increase the accuracy of the results but only leads in longer solution times.

4. COMPARISON BETWEEN EXPERIMENTAL AND NUMERICAL RESULTS

The criteria adopted to assess the efficiency of the proposed numerical model are:

- (i). The analysis should accurately capture the experimentally observed failure mode for all involved materials (i.e. concrete, internal reinforcement and SRG jacket).
- (ii). The numerical and experimental load-deflection curves should be similar. Towards this goal, five parameters were employed, namely, the maximum load (P_{max}), the ultimate load (P_u), the corresponding displacements (δ_{max}) and (δ_u), and the dissipated energy. The ultimate load is defined as the load at a 20 % drop of the peak load, whereas in the case that no descending branch appears in the load-deflection curve, the last point of the curve is considered as the ultimate. Dissipated energy is the area below the force-displacement diagram, measured in Joules (J). The error for each parameter (load, displacement or energy) was defined as the absolute value of the experimental result minus the corresponding numerical one, divided by the experimental value.

The following sections present the numerical results and make relevant comparisons with the corresponding experimental ones.

4.1 Failure modes

- Group A

The control specimen of Group A (specimen A0) failed in shear with a single inclined crack due to diagonal tension in its critical area. Numerical analysis has predicted an inclined shear crack similar to the experimental one (Figure 5). As the load gradually increased, the single crack expanded up to failure, simulating the experimental behavior. For the three retrofitted

specimens of Group A (AUH1, AFL1, AFH1), the numerical analysis predicted flexural failure since shear failure was suppressed by the addition of SRG jacketing. Thus, inelasticity was restricted to the bottom tensile face of the beams and the tensile reinforcement. Specifically, numerical analysis showed two main vertical flexural cracks below the load point, outside the retrofitted area, similar to the experimentally observed patterns. Yielding of the internal bottom steel reinforcement was also predicted, whereas the SRG jacket did not show any damage (i.e. slippage, debonding or fracture), a fact that is in accordance with the experimental results.

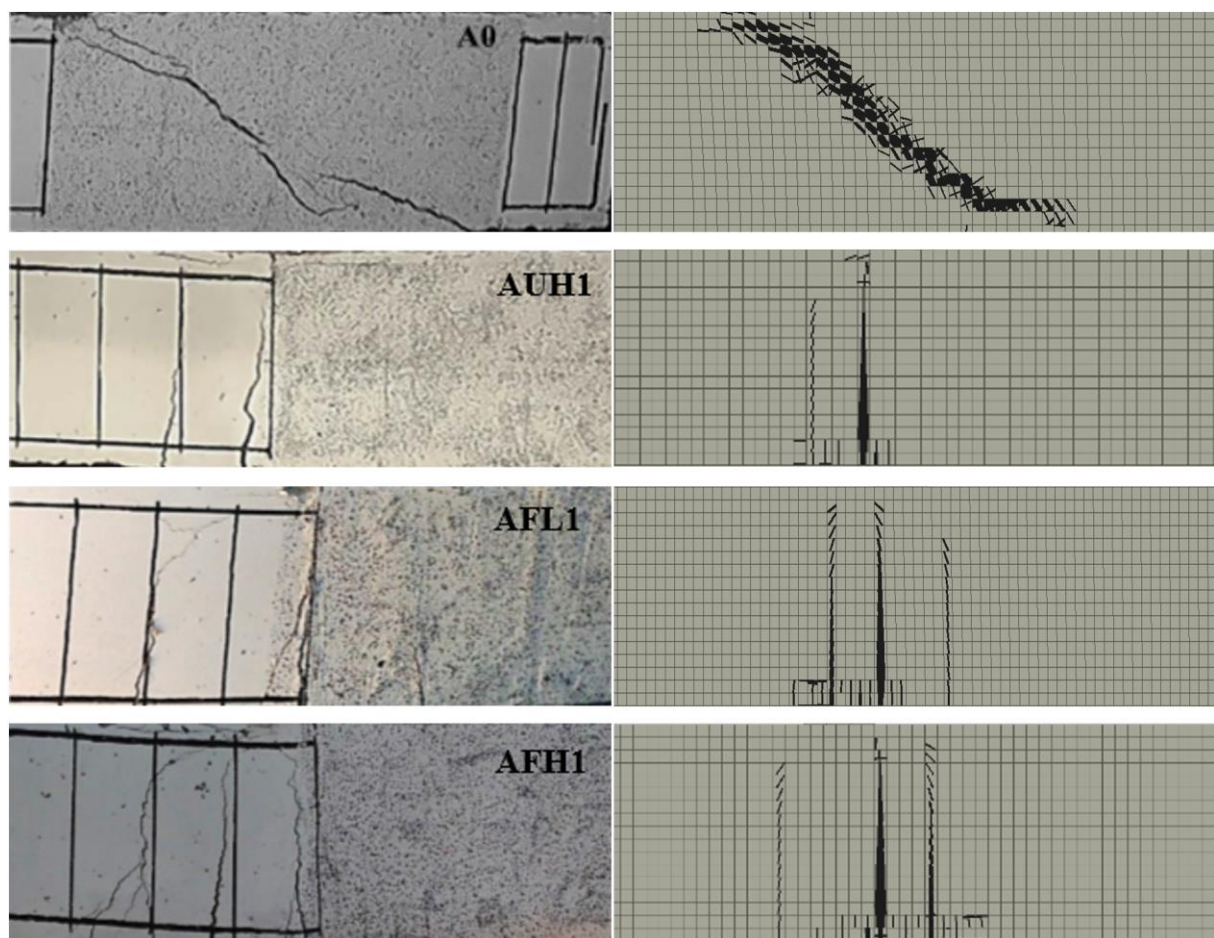


Figure 5. Experimental vs. numerical failure modes for Group A specimens.

- Group B

The control specimen of Group B (specimen B0) failed experimentally in shear, similarly to A0 and was again captured by numerical analysis (Figure 6). Specimens BUL1 and BUL2 retrofitted with one and two U-wrapped SRG jackets, respectively, failed again in shear, yet at

higher levels of loading, compared to the control specimen (B0). Numerical analysis correctly predicted the development of a single inclined shear crack in the retrofitted area of the beam similar to the experimental observations (Figure 6). The *fib* MC 2010 [44] bond-slip law accurately described the debonding of the SRG jacket, whereas no fracture of the steel cords was observed. It is worth mentioning that according to both numerical and experimental investigations, crack width increased dramatically after the detachment of the textile, eventually leading to the failure of the specimens. Contrariwise, specimens BFL1 and BFL2 strengthened with low-density fully-wrapped jackets of one and two layers, respectively, behaved in a ductile way; BFL1 demonstrated a combined shear and flexural failure mode. As seen in Figure 6, for specimen BFL1, both experimental and numerical crack patterns show diffused diagonal shear and flexural cracks in the critical area of the beam. Beam BFL2 failed due to flexure, with the overall crack pattern being similar to that of beam BFL1 (Figure 6). Both for BFL1 and BFL2 beams color contour indicates that the numerically estimated crack width is smaller compared to the previous specimens. This is attributed to the beneficial confinement action of the fully-wrapped jackets that limits the failure cracks and promotes the ductile response.

According to the numerical solution, both fully-wrapped specimens failed due to the tensile fracture of the steel cords, whereas no debonding was observed. This agrees with the experimental results and demonstrates that the zero-slip approach adopted for the fully-wrapped jackets was reasonable.

4.2 Comparison between numerical and experimental force-displacement response curves

The numerical force-displacement curves of Group A and B beams are compared to the corresponding experimental ones in Figures 7 and 9, respectively. The errors regarding maximum load (P_{\max}), ultimate load (P_u), maximum displacement (δ_{\max}), ultimate displacement

(δ_u), and absorbed energy are presented in detail in Table 3. Comparative plots between numerical and experimental results are presented in Figure 10.

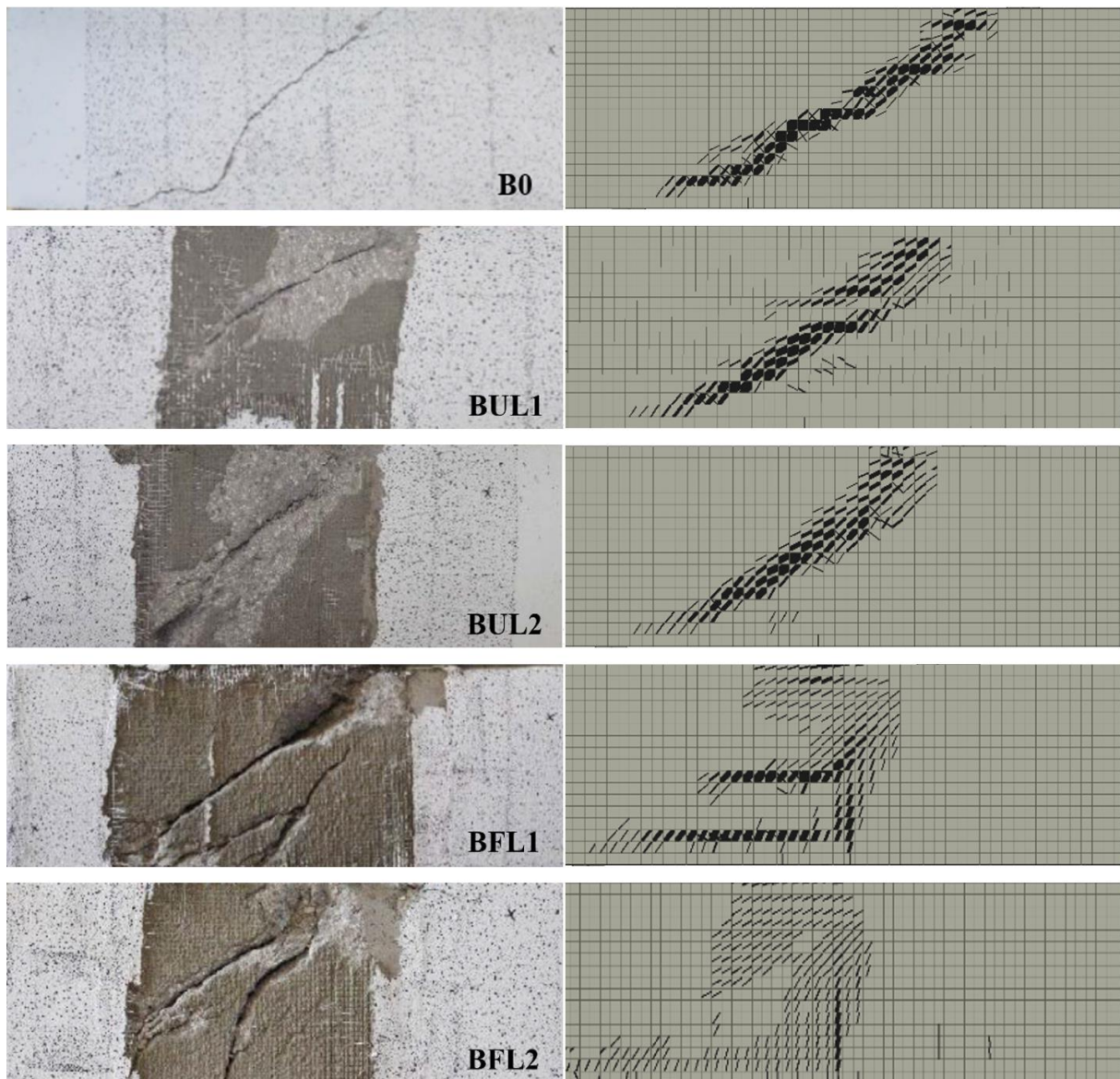


Figure 6. Experimental vs. numerical failure modes for Group B specimens.

- Group A

The control specimen of Group A (specimen A0) failed in shear. The numerical force-displacement curve is bilinear, with a single ascending branch up to peak strength, followed by an abruptly descending one. Jacketed specimens AUH1, AFL1, and AFH1 demonstrated similarly ductile force-displacement response curves. They reached a 30 % higher peak load

and a 330 % higher ultimate displacement compared to the control beam (A0). The numerical force-displacement curve comprised two parts; an initial up to the peak strength, and a second one, practically horizontal, reaching a displacement by 330 % higher compared to beam A0. It is noted that the high calculated error in δ_{max} of specimen AUH1 is misleading since it is only associated to the inclination of the post-elastic branch of the force-displacement curve. As seen in Figure 7, the numerical and experimental force-displacement curves are almost identical. However, the post-yielding branch of the experimental plot is perfectly plastic, whereas the corresponding branch of the numerical force-displacement curve has a mild hardening. This results to peak strength defined at two very different displacements, leading to this high displacement error value (88.5 %, Table 3).

The error in energy absorption, which is a more general indicator since it includes both force and displacement values, for specimens of group A was on average 4.12 % (Table 3 and Fig. 9).

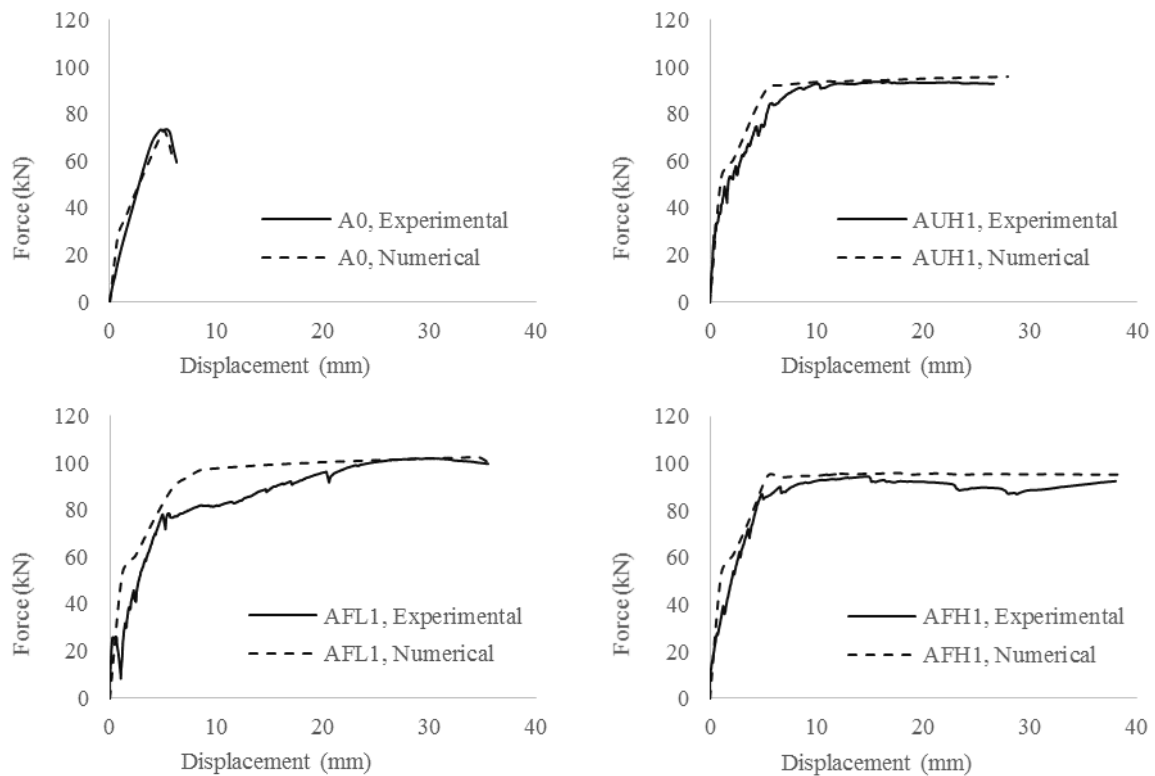


Figure 7. Comparison between experimental and numerical force-displacement curves for Group A specimens.

- Group B

The control specimen of Group B (Specimen B0) failed in shear, similarly to specimen A0. The bilinear force-displacement curve shows again an ascending branch up to peak strength, followed by an abruptly descending one (Figure 8). The small underestimation of the displacement at peak load (δ_{max}) may be attributed to the inability of modeling the dowel action of the longitudinal reinforcement, since 2-node truss elements, used to model steel reinforcement, operate only axially. Therefore, numerical analysis is unable to capture the experimentally observed load variation at the post-elastic branch of the force-displacement response curve, of specimen B0. This dowel action is more pronounced in specimen B0, compared to specimen A0, due to the higher percentage of longitudinal reinforcement.

Specimens BUL1 and BUL2 exhibited similarly brittle behavior, as illustrated in the numerical load-displacement diagram in Figure 8. The average strength and deformation capacity increase for both specimens was 107 % and 65 %, respectively. The numerical force-displacement curve comprises two branches; an ascending one up to the peak strength and an abruptly decreasing one to failure. According to both numerical and experimental investigations, strength drop occurred due to the detachment of the SRG jacket. The comparison between numerical and experimental force-displacement curves for specimens BUL1 and BUL2, as seen in Figure 8, shows good correlation, hence the adopted *fib* MC 2010 [44] bond law for modeling the SRG textile was adequate. The activation of bond slip function on individual strands showed a considerable slip up to about 2 mm with a similar debonding pattern to the experimental one, as shown in Figure 8.

Specimens BFL1 and BFL2 were strengthened with the low-density fully-wrapped jackets (one and two layers) performed in a more ductile manner. The ductile response is evident in the numerical load-displacement curve of Figure 9, where the post-elastic branch of the curve presents mild hardening. According to the numerical analysis, the average load and

deformation increase, for specimens BFL1 and BFL2, when compared to the control specimen of the group (B0), is equal to 140 % and 400 %, respectively. The displacement capacity increase is attributed to the use of fully-wrapped jackets, which provide effective confinement to the retrofitted area of the beam. Numerical analysis can predict the effect of confinement at full-scale provided that the calibration of the constitutive model is reasonable.

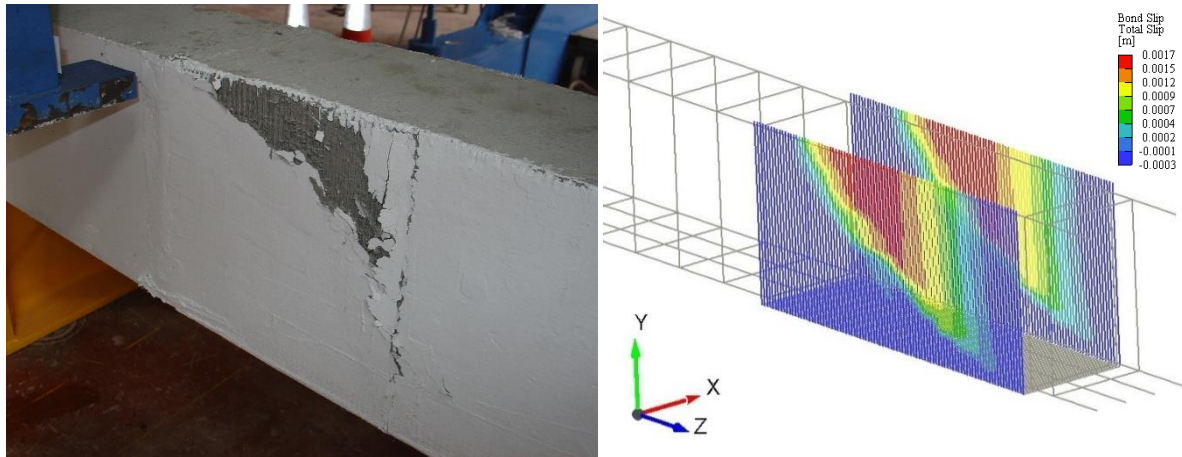


Figure 8. Comparison of debonding pattern between specimen BUL1 and numerical analysis.

For all specimens of group B, the 4.3 % average energy absorption error indicates that the numerical analysis predicted load and displacement capacity with high accuracy (Table 3 and Figure 10).

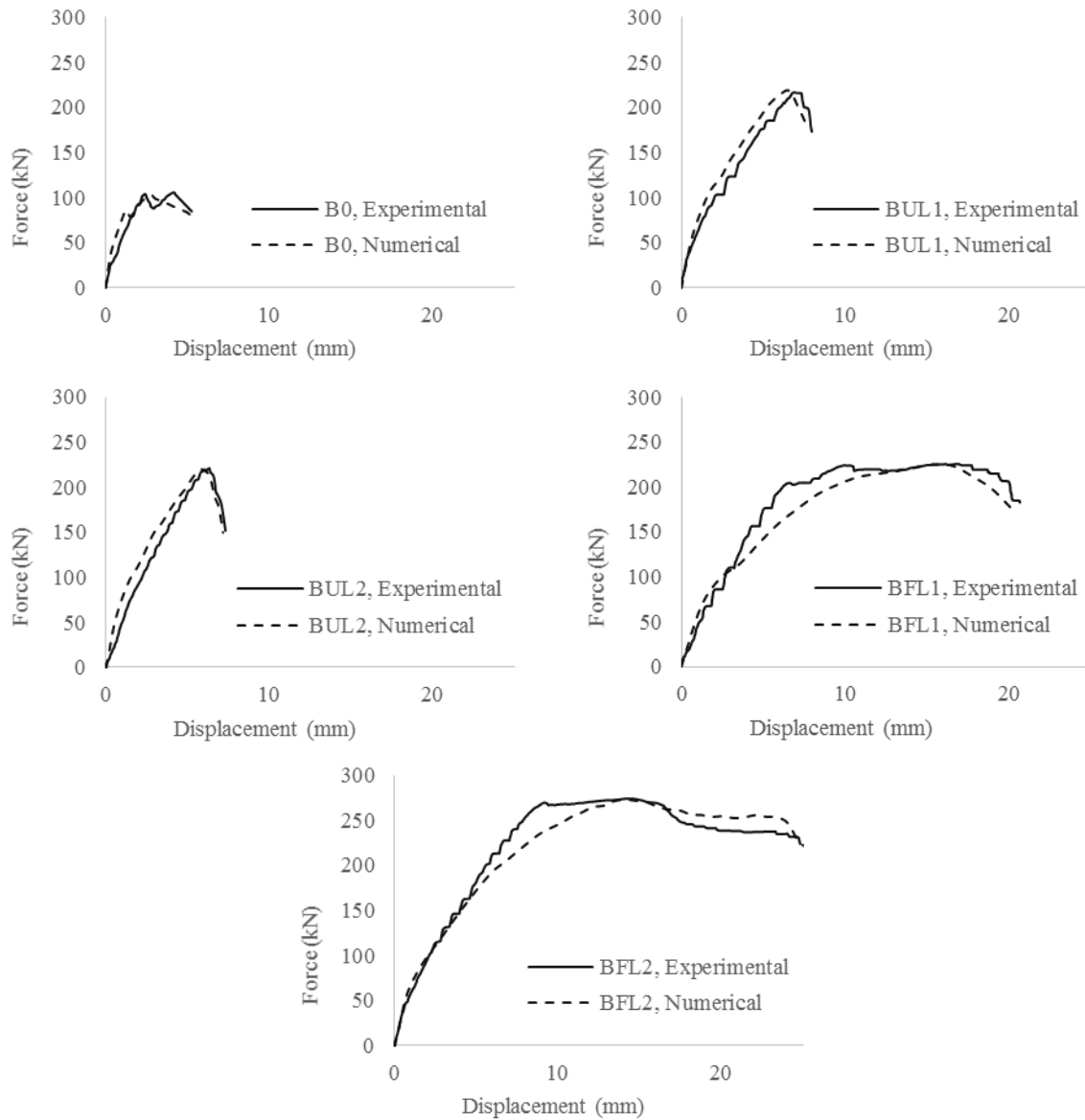


Figure 9. Comparison between experimental and numerical force-displacement curves for Group B specimens.

Table 3. Comparison between numerical and experimental results for all analyzed specimens in terms of failure modes and errors.

| Specimen | Beam failure mode | | SRG failure mode | | Load error | Displacement error | Dissipated energy error |
|-------------|-------------------|---------------|------------------|-------------|-------------------|-------------------------|-------------------------|
| | Num. | Exp. | Num. | Exp. | | | |
| A0 | Num. | Shear | Num. | - | P_{max} : 0.6 % | δ_{max} : 3.9 % | 1.8 % |
| | Exp. | Shear | Exp. | - | P_u : 0.6 % | δ_u : 4.2 % | |
| AUH1 | Num. | Flexure | Num. | No failure | P_{max} : 2.4 % | δ_{max} : 88.5 % | 6.2 % |
| | Exp. | Flexure | Exp. | No failure. | P_u : 0.9 % | δ_u : 17.7 % | |
| AFL1 | Num. | Flexure | Num. | No failure | P_{max} : 0.6 % | δ_{max} : 13.4 % | 3.3 % |
| | Exp. | Flexure | Exp. | No failure | P_u : 0.6 % | δ_u : 9.5 % | |
| AFH1 | Num. | Flexure | Num. | No failure | P_{max} : 1.2 % | δ_{max} : 11.0 % | 5.0 % |
| | Exp. | Flexure | Exp. | No failure | P_u : 1.2 % | δ_u : 4.2 % | |
| B0 | Num. | Shear | Num. | - | P_{max} : 1.5 % | δ_{max} : 33.7 % | 2.2 % |
| | Exp. | Shear | Exp. | - | P_u : 1.9 % | δ_u : 8.3 % | |
| BUL1 | Num. | Shear | Num. | Slip | P_{max} : 0.7 % | δ_{max} : 4.6 % | 3.3 % |
| | Exp. | Shear | Exp. | Slip | P_u : 1.7 % | δ_u : 2.8 % | |
| BUL2 | Num. | Shear | Num. | Slip | P_{max} : 0.4 % | δ_{max} : 7.7 % | 6.7 % |
| | Exp. | Shear | Exp. | Slip | P_u : 0.9 % | δ_u : 2.7 % | |
| BFL1 | Num. | Shear/Flexure | Num. | Fracture | P_{max} : 0.1 % | δ_{max} : 8.7 % | 8.1 % |
| | Exp. | Shear/Flexure | Exp. | Fracture | P_u : 0.1 % | δ_u : 2.8 % | |
| BFL2 | Num. | Flexure | Num. | Fracture | P_{max} : 0.5 % | δ_{max} : 2.5 % | 1.2 % |
| | Exp. | Flexure | Exp. | Fracture | P_u : 0.5 % | δ_u : 0.5 % | |

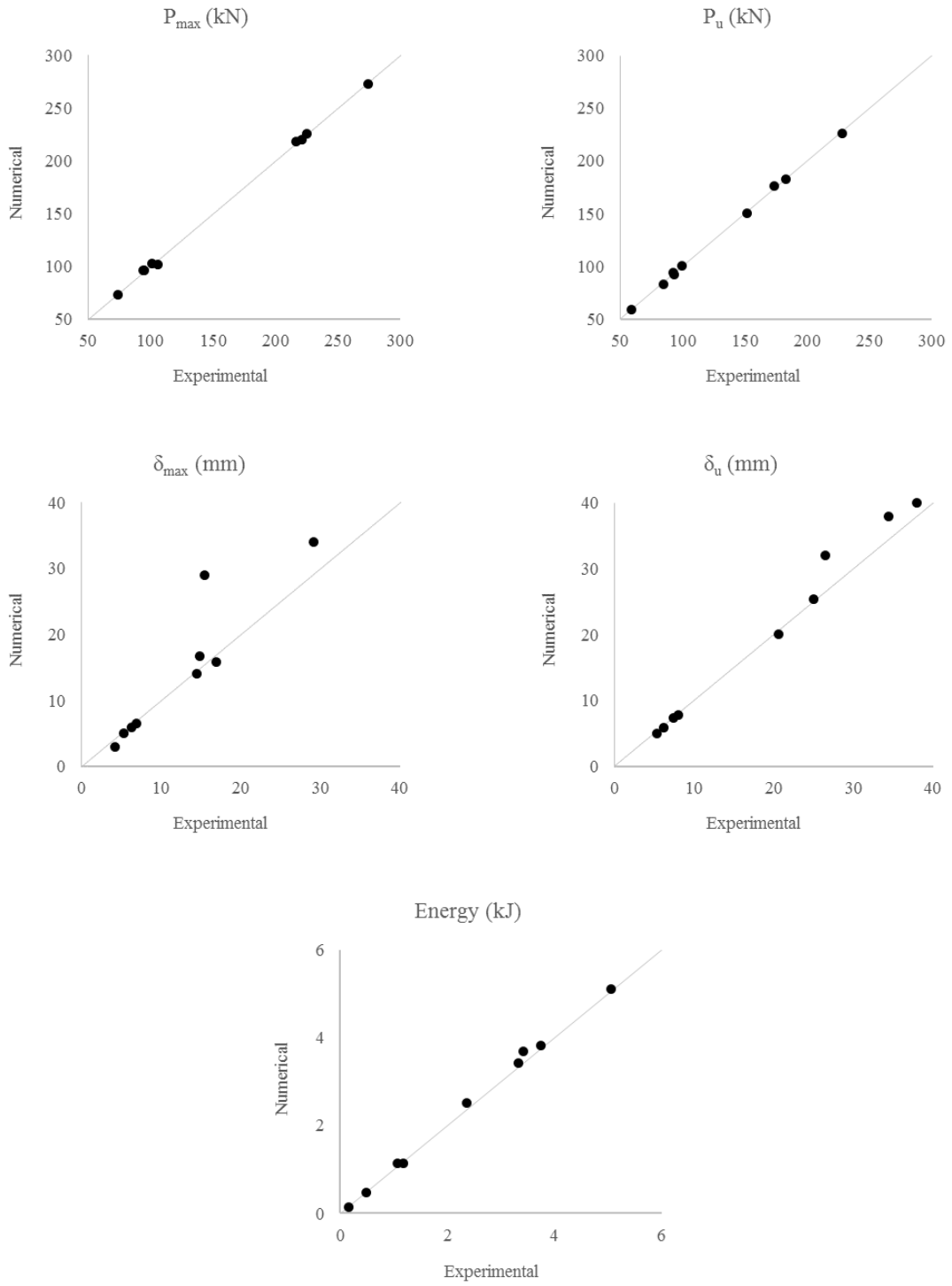


Figure 10. Numerical vs experimental plot for all specimens under various comparison parameters.

5. CONCLUSIONS

This paper presents a new approach for modeling shear deficient R/C beams strengthened with Steel Reinforced Grout (SRG) jackets. Embedded truss elements were employed to simulate both external steel cords and steel reinforcement, whereas concrete was modeled by three-dimensional solid elements. Experimental results of nine R/C beams were employed to assess the accuracy of the numerical methodology. They featured a variety of concrete strength, longitudinal steel reinforcement and jacketing schemes. Finite element analysis closely predicted the experimentally observed behavior of control and the retrofitted specimens, as well as their force-displacement curves. The following main conclusions are drawn:

- The numerical analysis successfully predicted the failure modes and the corresponding crack patterns of all tested beams. Specifically, in case of the fully-wrapped beams, the use of full-bond conditions for the steel cords embedded in the mortar allowed for the prediction of the experimentally observed behavior where tensile fracture of the steel cords occurred. In case of U-wrapped jackets, the use of a bond-slip law, here the *fib* MC 2010 [44], allowed slippage of the cords within the mortar matrix to occur, thus predicting the debonding failure mode of the textile.
- The numerical analysis captured the response of the longitudinal steel reinforcement sufficiently. This was not the case in control specimen B0 due to the dowel action of the longitudinal reinforcement which could not be reproduced by the truss elements used in the numerical model.
- The load error was, on average, less than 1%. This minor difference suggests that the modeling approach and calibration of concrete constitutive law were sufficiently accurate.

- The displacement error was, on average, less than 10%. The only exception was δ_{\max} for specimen AUH1 with an error of 89 % attributed to the difference in the definition of the peak strength.
- The correlation between numerical and experimental energy absorption was satisfying with an average error of 4.2%.
- The time-efficiency of the proposed finite element methodology was evaluated through trial analyses. Using embedded truss elements to model steel cords, instead of the usually suggested two-dimensional elements, resulted in 80% reduction of the solution time. This time-efficiency is directly linked to the reduction of the utilized number and dimension of finite elements.

Overall, the present study proposes an efficient numerical approach for simulating the response of shear-deficient R/C beams, strengthened with SRG jackets. Future research will include further applications of the suggested approach on published experimental studies (e.g. [31,32,48], together with comparisons to more measured response parameters (where available) and further refinement of the employed bond-slip law in the case of U-wrapping.

REFERENCES

- [1] Bakis C.E., Bank L.C., Brown V.L., Cosenza E., Davalos J.F., Lesko J.J., Machida A., Rizkalla S.H. and Triantafillou T.C. (2002) “Fiber-Reinforced Polymer Composites for Construction – State-of-the-Art Review” Journal of composites for construction DOI: 10.1061/(ASCE)1090-0268(2002)6:2(73)
- [2] Triantafillou T.C. (1998) “Shear Strengthening of Reinforced Concrete Beams Using Epoxy-Bonded FRP Composites” ACI Structural Journal, 95, 107-115
- [3] Triantafillou T.C., Choutopoulou E., Fotaki E., Skorda M., Stathopoulou M., Karlos K. (2015) “FRP confinement of wall-like reinforced concrete columns” Materials and Structures DOI 10.1617/s11527-015-0526-5
- [4] Triantafillou T.C., Deskovic N., Deuring M. (1992) “Strengthening of Concrete Structures with Prestressed Fiber Reinforced Plastic Sheets” ACI Structural Journal, Title no. 89-S22
- [5] Triantafillou T.C., Plevris N. (1992) “Strengthening of RC beams with epoxy-bonded fibre-composite materials” Materials and Structures, 1992, 25, 201-211

- [6] Tastani S.P., Pantazopoulou S.J., Zdoumba D., Plakantaras V., Akritidis E. (2006) "Limitations of FRP Jacketing in Confining Old-Type Reinforced Concrete Members in Axial Compression" *Journal of Composites for Construction* DOI: 10.1061/ASCE1090-0268(2006)10:1(13)
- [7] Pantazopoulou S., Tastani S., Thermou G., Triantafillou T., Monti G., Bournas D., Guadagnini M. (2016) "Background to the European seismic design provisions for retrofitting RC elements using FRP materials" *Structural Concrete*, Ernst & Sohn, DOI: 10.1002/suco.201500102
- [8] Ma G., Li H. (2015) "Experimental Study of the Seismic Behavior of Predamaged Reinforced-Concrete Columns Retrofitted with Basalt Fiber-Reinforced Polymer" *J. Compos. Constr.*, 2015, 19(6): 04015016
- [9] Lau D., Qiu Q., Zhou A., Chow C.L. (2016) "Long term performance and fire safety aspect of FRP composited used in building structures" *Construction and Building Materials* 126 (2016) 573–585
- [10] Koutas L. and Triantafillou T.C. (2013) "Use of Anchors in Shear Strengthening of Reinforced Concrete T-Beams with FRP" *Journal of Composites for Construction* 2013.17:101-107.
- [11] Karatzikis M., Papanicolaou C.G., Antonopoulos C.P. and Triantafillou T.C. (2005) "Experimental Investigation of Nonconventional Confinement for Concrete Using FRP" *Journal of Composites for Construction* DOI: 10.1061/(ASCE)1090-0268(2005)9:6(480)
- [12] Antonopoulos C.P. and Triantafillou T.C. (2003) "Experimental Investigation of FRP-Strengthened RC Beam-Column Joints" *Journal of Composites for Construction* DOI: 10.1061/(ASCE)1090-0268(2003)7:1(39)
- [13] Thermou, G.E., and Hajirasouliha, I. (2018b) "Design-oriented models for concrete columns confined by steel-reinforced grout jackets" *Construction and Building Materials*, 178, 313-326.
- [14] Triantafillou T.C., Papanicolaou C.G., Zissimopoulos P, Laourdekis T. "Concrete confinement with textile-reinforced mortar jackets" *ACI Struct J* 2006; 103(1): 28-37.
- [15] Koutas L.N., Bournas D.A. (2016) "Flexural Strengthening of Two-Way RC Slabs with Textile-Reinforced Mortar: Experimental Investigation and Design Equations" *Journal of Composites for Construction* DOI: 10.1061/(ASCE)CC.1943-5614.0000713.
- [16] Tetta Z.C., Koutas L.N., Bournas D.A. (2015) "Textile-reinforced mortar (TRM) versus fiber-reinforced polymers (FRP) in shear strengthening of concrete beams" *Composites Part B: Engineering* <https://doi.org/10.1016/j.compositesb.2015.03.055>
- [17] Koutas L., Triantafillou T.C. (2013) "Use of Anchors in Shear Strengthening of Reinforced Concrete T-Beams with FRP" *Journal of Composites for Construction* DOI:10.1061/(ASCE)CC.1943-5614.0000316.
- [18] Tetta Z.C., Koutas L.N., Bournas D.A. (2016) "Shear strengthening of full-scale RC T-beams using textile-reinforced mortar and textile-based anchors" *Composites Part B: Engineering* <https://doi.org/10.1016/j.compositesb.2016.03.076>
- [19] Raoof S.M., Koutas L.N., Bournas D.A. (2017) "Textile-reinforced mortar (TRM) versus fibre-reinforced polymers (FRP) in flexural strengthening of RC beams" *Construction and Building Materials* <https://doi.org/10.1016/j.conbuildmat.2017.05.023>
- [20] Raoof S.M., Koutas L.N., Bournas D.A. (2016) "Bond between textile-reinforced mortar (TRM) and concrete substrates: Experimental investigation" *Composites Part B: Engineering* <https://doi.org/10.1016/j.compositesb.2016.05.041>

- [21] Bournas D.A., Lontou P.V., Papanicolaou C.G., Triantafillou T.C. (2007) “Textile-Reinforced Mortar versus Fiber-Reinforced Polymer Confinement in Reinforced Concrete Columns” *ACI Structural Journal*, 104-S70
- [22] Koutas L.N., Tetta Z., Bournas D.A., Triantafillou T.C. (2019) “Strengthening of Concrete Structures with Textile Reinforced Mortars: State-of-the-Art Review” *Journal of Composites for Construction* DOI: 10.1061/(ASCE)CC.1943-5614.0000882
- [23] Thermou, G.E., Pantazopoulou, S. (2007) “Metallic fabric jackets: an innovative method for seismic retrofitting of substandard RC prismatic members” *Structural Concrete, fib*, pp. 35-46
- [24] Thermou G.E., Katakalos K., Manos G. (2014) “Concrete confinement with steel-reinforced grout jackets” *Materials and Structures* DOI 10.1617/s11527-013-0239-6
- [25] Thermou G.E., Katakalos K., Manos G. (2015) “Influence of the cross section shape on the behaviour of SRG-confined prismatic concrete specimens” *Materials and Structures* DOI 10.1617/s11527-015-0545-2
- [26] Thermou G.E., Katakalos K., Alexiou G. (2016) “SRG jacketing of short RC columns: Experimental investigation” *Greek Conference on Concrete Structures*, Thessaloniki, November 2016
- [27] Thermou G.E., Katakalos K., Manos G. (2017) “Experimental investigation of substandard RC columns confined with SRG jackets under compression” *Composite Structures* DOI:10.1016/j.compstruct.2017.09.082
- [28] Thermou G.E., Papanikolaou V.K., Hajirasouliha I. (2018a) “A Novel Method for Seismic Retrofitting of Substandard RC Columns using Steel-Reinforced Grout jacketing” *16th European Conference on Earthquake Engineering*, Thessaloniki 2018
- [29] Thermou, G.E., and Hajirasouliha, I. (2018b) “Compressive behaviour of concrete columns confined with steel reinforced grout jackets” *Composites Part B: Engineering Journal*, 138, 222-23.
- [30] Thermou G.E., Papanikolaou V.K., Lioupis C., Hajirasouliha (2019) “Steel-Reinforced Grout (SRG) strengthening of shear-critical RC beams” *Construction and Building Materials* <https://doi.org/10.1016/j.conbuildmat.2019.04.259>
- [31] Gonzalez-Libreros J.H., Sneed L.H., D’Antino T.D., Pellegrino C. (2017) “Behavior of RC beams strengthened in shear with FRP and FRCM composites” *Engineering Structures* 150 (2017) 830–842
- [32] Wakjira G.T., Ebead U. (2019) “Experimental and analytical study on strengthening of reinforced concrete T-beams in shear using steel reinforced grout (SRG)” *Composites Part B* 177 (2019) 107368
- [33] Napoli A., Realfonzo R., Petracca M., Candeloro F., Camata G., Casadei P. (2016) “Flexural strengthening of RC slabs with SRP/SRG: an experimental-numerical comparison” *Applied Mechanics and Materials* doi:10.4028/www.scientific.net/AMM.847.381
- [34] ACI 549.4R-13: Guide to Design and Construction of Externally Bonded Fibre-Reinforced Cementitious Matrix (FRCM) Systems for Repair and Strengthening Concrete and Masonry Structures, ACI Committee 549
- [35] Bencardino F. and Condello A. (2016) “3D FE Analysis of RC Beams Externally Strengthened with SRG/SRP Systems” *MDPI Fibers* 2016 4, 19 doi:10.3390/fib4020019

- [36] Yuan H., Lu X., Hui D., Feo L. (2012) “Studies on FRP-concrete interface with hardening and softening bond-slip law” *Composite Structures* <https://doi.org/10.1016/j.compstruct.2012.06.009>
- [37] Cervenka Consulting (2018) “ATENA Program Documentation”, Prague, Czech Republic.
- [38] Červenka V., Jendele L., Červenka J. (2018) “Theory” ATENA Program Documentation Part 1, Červenka Consulting, Prague, Czech Republic.
- [39] Sajdlová T. (2016) “ATENA Science – GiD Strengthening of concrete structures” ATENA Program Documentation Part 4-9, Červenka Consulting, Prague.
- [40] Papanikolaou V.K. (2007) “Analytical Study of Confined Reinforced Concrete Members using the Three-Dimensional Nonlinear Finite Element Method” PhD Thesis, Aristotle University of Thessaloniki, Greece
- [41] Papanikolaou V.K., Kappos A.J. (2009) “Numerical study of confinement effectiveness in solid and hollow reinforced concrete bridge piers: Analysis results and discussion” *Computers and Structures* doi:10.1016/j.compstruc.2009.05.005
- [42] Papanikolaou V.K., Kappos A.J. (2009) “Numerical study of confinement effectiveness in solid and hollow reinforced concrete bridge piers: Methodology” *Computers and Structures* doi:10.1016/j.compstruc.2009.05.004
- [43] Papanikolaou, V., Kappos, A. (2005) “Modeling Confinement in Concrete Columns and Bridge Piers through 3D Nonlinear Finite Element Analysis” fib Symposium “Keep Concrete Attractive”, Budapest 2005
- [44] CEB-FIP Model Code 2010 (2010), Thomas Telford Ltd., London, 978-0-7277-1696-5
- [45] Cervenka J. and Cervenka V. (1999) “Three Dimensional Combined Fracture-Plastic Material Model for Concrete” Proceedings of the 5th US National Congress on Computational Mechanics, Boulder, CO.
- [46] Menétrey, P. and Willam K.J. (1995) “Triaxial Failure Criterion for Concrete and its Generalization”, *ACI Structural Journal*, Vol. 92, No. 3, pp. 311-318.
- [47] Schenk O., Gärtner K., Fichtner W. and Stricker A. (2001) “PARDISO: a high-performance serial and parallel sparse linear solver in semiconductor device simulation” *Future Generation Computer Systems*, Volume 18, Issue 1, P 69-78, ISSN 0167-739X, [https://doi.org/10.1016/S0167-739X\(00\)00076-5](https://doi.org/10.1016/S0167-739X(00)00076-5).
- [48] Wakjira G.T., Ebead U. (2020) “Shear span-to-depth ratio effect on steel reinforced grout strengthened reinforced concrete beams” *Engineering Structures* 216 (2020) 11037